7
Estimation of magnetisation direction from axial magnetic field component and gradient tensor element ratios of a dipole source

C.A. Foss, K.B. McKenzie and D.A. Clark

ABSTRACT

Anomalies in the measured magnetic field mark the location of subsurface magnetisations. We show that using a dipole model the direction of the contrast of that magnetisation against the surrounding material can be estimated by analysis of the components or tensor gradients of the magnetic field directly above the magnetisation. We propose the use of the normalised source strength (NSS) as an appropriate method to locate the centre of magnetisation and show that the NSS is superior to the total gradient (TG) that has traditionally been used for this application. Imperfections in applying the analysis arise from imprecision in locating the centre of magnetisation and inaccuracies in assigning a dipole model to represent non-dipole magnetisations. We investigate the effect of non-dipole characteristics according to the shape of the distribution of magnetisation, any plunge of that distribution, and the distance at which the magnetic field is measured. Finally, we show that for a magnetic field anomaly measured in Queensland, Australia the NSS peak coincides with the centre of magnetisation estimated by parametric inversion, and that magnetisation direction estimates made independently by tensor analysis and inversion agree to within 5°. For this anomaly the TG peak is significantly displaced from the centre of the inversion model and the direction of magnetisation estimated by tensor analysis at the TG peak differs from the inversion direction by 38°.

7.1 INTRODUCTION

The external magnetic field of a source body is a function of its resultant (induced plus remanent) magnetisations. Helbig (1963) provides a proof that over an extensive horizontal surface the direction of magnetisation of a compact source can be recovered from integral moments of the magnetic field components about the point directly above its centre. Helbig analysis itself provides a practical methodology to recover source magnetisation estimates from measured magnetic fields (Schmidt and Clark 1998; Phillips 2005; Phillips *et al.* 2007; Caratori Tontini and Pedersen 2008; Clark 2014) but the magnetic component moment integrals are highly sensitive to imperfection in removing background fields. The analysis requires isolation of the field due to the source and provision of the horizontal centre of magnetisation. Magnetic field components are derived by FFT phase transforms from a TMI grid (Lourenço and Morrison 1973; Purucker 1990; Blakely 1995; Schmidt and Clark 1998; Clark 2013). Phillips *et al.* (2007) provided an approximate relationship to use derivatives of

the field components and reduce dependence on isolation from background fields. Many other methods have been established to estimate magnetisation direction from magnetic field data (Fedi *et al.* 1994; Dannemiller and Li 2006; McKenzie *et al*. 2012) including parametric inversion (Foss 2006; Foss and McKenzie 2011; Pratt *et al*. 2014) and voxel inversion (Paine *et al*. 2001; Lelièvre and Oldenburg 2009; Fullagar and Pears 2015; Li 2012).

Here we propose an approximate method to estimate the magnetisation direction of moderately compact sources from the ratios of their magnetic field components or tensor gradient elements directly above their centres. We first apply the NSS transform to a TMI grid and select suitable near-circular NSS anomalies. At the centre points of those anomalies we sample the Cartesian components of the field and/or its tensor gradient elements derived from FFT of the measured TMI field. Component analysis of measured fields requires that anomalies are separated from the background field (a regional-residual separation) but this is generally not required for tensor analysis because the anomalous field contributions tend to be the dominant local field gradients. Conversely, short wavelength variations due to measurement imperfections or near-surface magnetisations can be disruptive to gradient analysis and may require pre-processing such as by a mild upward continuation. The NSS derivation is complex and computationally intense but can be applied either to complete multi-anomaly field sets or to individual anomaly separations. We also include comparison of analyses performed at locations where the total gradient is a maximum.

7.2 ANALYTICAL BASIS OF THE FIELD COMPONENT RATIO METHOD

The expression for the magnetic field vector $\mathbf{B}(\mathbf{r})$ at an observation point $\mathbf{r} = (x, y, z)^T$ due to a point dipole source possessing a magnetic moment $\mathbf{m}$ and located at the origin is given by Blakely (1995, p. 75) as:

$$\mathbf{B}(\mathbf{r}) = \frac{C_m}{r^3}\{3(\mathbf{m}\cdot\hat{\mathbf{u}}_\mathbf{r})\,\hat{\mathbf{u}}_\mathbf{r} - \mathbf{m}\}, \text{ (Eqn 7.1)}$$

where $\hat{\mathbf{u}}_\mathbf{r}$ is the unit vector in the direction of the line joining the dipole to the measurement point $\mathbf{r}$

$$\hat{\mathbf{u}}_\mathbf{r} = \left(u_{rx}, u_{ry}, u_{rz}\right)^T = \left(\frac{x}{r}, \frac{y}{r}, \frac{z}{r}\right)^T ; r = |\mathbf{r}| = \sqrt{x^2+y^2+z^2}.$$

and where C_m is a constant which depends on the system of electromagnetic units used (see Blakely 1995, pp. 67–68). In the International Standard (SI) system of units, C_m = 100 nH/m or 100 nTm/A for magnetic fields expressed in nanotesla (nT) and magnetisations expressed in ampere per metre (A/m). The coordinate system adopted here follows the International Geomagnetic Reference Field convention, i.e. *x* is North, y is East and +z is vertically down. The Cartesian components of the magnetic field vector are

$$B_x(\mathbf{r}) = \frac{C_m}{r^3}\{3(\mathbf{m}\cdot\hat{\mathbf{u}}_\mathbf{r})u_{rx} - m_x\}$$
$$= \frac{C_m}{r^3}\left\{3\left(\frac{m_x x^2}{r^2} + \frac{m_y xy}{r^2} + \frac{m_z xz}{r^2}\right) - m_x\right\}, \text{ (Eqn 7.2)}$$

$$B_y(\mathbf{r}) = \frac{C_m}{r^3}\{3(\mathbf{m}\cdot\hat{\mathbf{u}}_\mathbf{r})u_{ry} - m_y\}$$
$$= \frac{C_m}{r^3}\left\{3\left(\frac{m_x xy}{r^2} + \frac{m_y y^2}{r^2} + \frac{m_z yz}{r^2}\right) - m_y\right\}, \text{ (Eqn 7.3)}$$

$$B_z(\mathbf{r}) = \frac{C_m}{r^3}\{3(\mathbf{m}\cdot\hat{\mathbf{u}}_\mathbf{r})u_{rz} - m_z\}$$
$$= \frac{C_m}{r^3}\left\{3\left(\frac{m_x xz}{r^2} + \frac{m_y yz}{r^2} + \frac{m_z z^2}{r^2}\right) - m_z\right\}. \text{ (Eqn 7.4)}$$

The expressions in Eqns 7.2–7.4 for the magnetic field components due to a point dipole or uniformly magnetised sphere are completely general and apply to any external observation point. However, for an observation station located at a height *z* directly above the dipole or above the centre of a magnetised sphere, the expressions for the magnetic field components become greatly simplified since $\hat{\mathbf{u}}_\mathbf{r} = (0, 0, -1)^T$. Thus

$$B_x(0,,0,\text{-}z) = -\frac{C_m m_x}{r^3}.; B_y(0,,0,\text{-}z) = -\frac{C_m m_y}{r^3}.; \text{ and}$$

$$B_z(0,,0,\text{-}z) = \frac{C_m m_z}{r^3}\left[\frac{3z^2}{r^2} - 1\right] = \frac{2C_m m_z}{r^3}.$$

The corresponding expressions for the magnetic field components produced by a magnetised sphere of radius *a*, volume *v*, magnetisation $\mathbf{M}$ and magnetic moment $\mathbf{m} = \mathbf{M}v$ are

$$B_x(0,,0,\text{-}z) = -\frac{C_m m_x}{r^3} = -\frac{C_m M_x v}{r^3} = -\left(\frac{4\pi}{3}\right)\frac{C_m M_x a^3}{r^3}.$$
(Eqn 7.5)

$$B_y(0,0,\text{-}z) = -\frac{C_m m_y}{r^3} = -\frac{C_m M_y v}{r^3} = -\left(\frac{4\pi}{3}\right)\frac{C_m M_y a^3}{r^3}.$$
(Eqn 7.6)

$$B_z(0,0,\text{-}z) = -\frac{2C_m m_z}{r^3} = \frac{2C_m M_z v}{r^3} = \left(\frac{8\pi}{3}\right)\frac{C_m M_z a^3}{r^3}.$$
(Eqn 7.7)

By inspection of Eqns 7.5 and 7.6, an expression for the declination of magnetisation D_M (or declination of magnetic moment) at any point $\mathbf{r} = (0,0,-z)^T$ above the point dipole or centre of a magnetised sphere is obtained from the ratio of the horizontal field components, namely,

$$D_M = \arctan\left(\frac{M_y}{M_x}\right) = \arctan\left(\frac{-B_y}{-B_x}\right) \quad \text{for } 0 \le D_M \le 2\pi.$$

(Eqn 7.8)

Similarly, by inspection of Eqns 7.5–7.7, the inclination of magnetisation I_M is obtained from the ratio of the horizontal field component to half the vertical field component, namely,

$$I_M = \arctan\left(\frac{M_z}{M_h}\right) = \arctan\left(\frac{B_z}{2\sqrt{B_x^2 + B_y^2}}\right) \quad \text{for } -\frac{\pi}{2} \le I_M \le \frac{\pi}{2}.$$

(Eqn 7.9)

The expression for the magnetic gradient tensor at a measurement point $\mathbf{r} = (x, y, z)^T$ due to a point dipole with magnetic moment $\mathbf{m}$ centred at the origin is given by Wynn *et al.* (1975) and Wilson (1985), namely,

$$B_{ij}(\mathbf{r}) = u_{ri}\mu_j + u_{rj}\mu_i + (\boldsymbol{\mu}\cdot\hat{\mathbf{u}}_\mathbf{r})\delta_{ij} - 5(\boldsymbol{\mu}\cdot\hat{\mathbf{u}}_\mathbf{r})u_{ri}u_{rj} \quad \text{(Eqn 7.10)}$$

for i,j = 1,2,3 or x,y,z and where $\boldsymbol{\mu} = (\mu_x, \mu_y\ \mu_z)^T$ is the scaled magnetic moment and δ_{ij} is Kronecker delta.

For a uniformly magnetised sphere of radius a, volume v and magnetisation $\mathbf{M}$, the scaled magnetic moment $\boldsymbol{\mu}(\mathbf{r})$ is

$$\boldsymbol{\mu}(\mathbf{r}) = \frac{3\mathrm{C_m}\mathbf{m}}{r^4} = \frac{3\mathrm{C_m}\mathbf{M}\mathrm{v}}{r^4} = \frac{4\pi\mathrm{C_m}a^3\mathbf{M}}{r^4}, \quad \text{(Eqn 7.11)}$$

The expressions in Eqns 7.10 and 7.11 for the gradient tensor due to a dipole or uniformly magnetised sphere are completely general and apply to any external observation point. However, for an observation station P(0, 0, −z) located at a height |z| directly above a point dipole or magnetised sphere centred at the origin, the expressions for its gradient tensor become greatly simplified since $\hat{\mathbf{u}}_\mathbf{r} = (u_{rx}, u_{ry}, u_{rz})^T = (0,0,-1)^T$. Hence all terms in Eqn 7.10 not involving u_{rz} are identically zero. Therefore, at any observation station $\mathbf{r} = (0, 0, -z)^T$, the elements of the gradient tensor $B_{ij}(\mathbf{r})$ are

$$B_{xx} = B_{11} = \left(\boldsymbol{\mu}\cdot\hat{\mathbf{u}}_\mathbf{r}\right)\delta_{11} = -\mu_z = -\frac{4\pi\mathrm{C_m}a^3}{r^4}M_z. \quad \text{(Eqn 7.12)}$$

$$B_{xy} = B_{12} = 0. \quad \text{(Eqn 7.13)}$$

$$B_{xz} = B_{13} = u_{r3}\mu_1 = -\mu_x = -\frac{4\pi\mathrm{C_m}a^3}{r^4}M_x. \quad \text{(Eqn 7.14)}$$

$$B_{yx} = B_{21} = 0 = B_{xy}. \quad \text{(Eqn 7.15)}$$

$$B_{yy} = B_{22} = (\boldsymbol{\mu}\cdot\hat{\mathbf{u}}_\mathbf{r})\delta_{22} = -\mu_z = -\frac{4\pi\mathrm{C_m}a^3}{r^4}M_z. \quad \text{(Eqn 7.16)}$$

$$B_{yz} = B_{23} = u_{r3}\mu_2 = -\mu_y = -\frac{4\pi\mathrm{C_m}a^3}{r^4}M_y. \quad \text{(Eqn 7.17)}$$

$$B_{zx} = B_{31} = u_{r3}\mu_1 = -\mu_x = -\frac{4\pi\mathrm{C_m}a^3}{r^4}M_x = B_{xz}.$$

(Eqn 7.18)

$$B_{zy} = B_{32} = u_{r3}\mu_2 = -\mu_y = -\frac{4\pi\mathrm{C_m}a^3}{r^4}M_y = B_{yz}.$$

(Eqn 7.19)

$$\begin{aligned} B_{zz} = B_{33} &= 2u_{r3}\mu_3 + (\boldsymbol{\mu}\cdot\hat{\mathbf{u}}_\mathbf{r})\delta_{33} - 5(\boldsymbol{\mu}\cdot\hat{\mathbf{u}}_\mathbf{r})u_{r3}^2 = \\ &= -2\mu_3 + (-\mu_3)\delta_{33} - 5(-\mu_3)u_{r3}^2 \\ &= -3\mu_3 + 5\mu_3 = 2\mu_3 = 2\mu_z = \frac{8\pi\mathrm{C_m}a^3}{r^4}M_z. \end{aligned} \quad \text{(Eqn 7.20)}$$

Hence the magnetic gradient tensor B_{ij} (0, 0, −z) is

$$\begin{aligned} \mathbf{B}(0,0,z) &= \begin{bmatrix} B_{xx} & B_{xy} & B_{xx} \\ B_{xy} & B_{yy} & B_{yz} \\ B_{zx} & B_{zy} & B_{zz} \end{bmatrix} \\ &= \frac{4\pi\mathrm{C_m}a^3}{r^4}\begin{bmatrix} -M_z & 0 & -M_x \\ 0 & -M_z & -M_y \\ -M_x & -M_y & 2M_z \end{bmatrix}. \end{aligned} \quad \text{(Eqn 7.21)}$$

By inspection of Eqns 7.14 and 7.17, the declination of magnetisation D_M at any point above the point dipole or centre of a magnetised sphere (for |z| > a) is obtained from the ratio of the B_{xz} and B_{yz} tensor elements as follows:

$$D_M = \arctan\left(\frac{M_y}{M_x}\right) = \arctan\left(\frac{-B_{yz}}{-B_{xz}}\right) \quad \text{for } 0 \le D_M \le 2\pi.$$

(Eqn 7.22)

Similarly, by inspection of Eqns 7.14, 7.17 and 7.20, the inclination of magnetisation I_M at any point above the point dipole or centre of the magnetised sphere is derived from the B_{xz}, B_{yz} and B_{zz} tensor elements as follows:

$$I_M = \arctan\left(\frac{M_z}{M_h}\right) = \arctan\left(\frac{B_{zz}}{2\sqrt{B_{xz}^2 + B_{yz}^2}}\right) \quad \text{for } -\frac{\pi}{2} \le I_M \le \frac{\pi}{2}.$$

(Eqn 7.23)

In this study we use peaks in both the normalised source strength (NSS) and total gradient (TG) to estimate the horizontal centre of magnetisation. As proposed by Beiki *et al.* (2012) and Clark (2012) the NSS is a generalisation of the scaled or normalised magnetic moment of a dipole source (Wynn *et al.* 1975; Wilson 1985). Denoted

by μ, the NSS is defined in terms of the eigenvalues of its magnetic gradient tensor, namely,

$$\mu = \sqrt{-\lambda_2^2 - \lambda_1\lambda_3} \qquad \text{for} \quad \lambda_1 \geq \lambda_2 \geq \lambda_3, \quad \text{(Eqn 7.24)}$$

where $\lambda_1 > 0$ is the first eigenvalue which is always positive, λ_2 is the second or intermediate eigenvalue which has the smallest absolute value and $\lambda_3 < 0$ is always negative. The traceless property of the tensor, together with the ordering of its eigenvalues, ensures that the NSS is always real and positive definite. Importantly, Clark (2012) and Beiki *et al.* (2012) showed that the NSS peaks directly over the source for several useful elementary models and that it is completely independent of magnetisation direction for arbitrary two-dimensional sources, as well as for spheres and axially magnetised narrow plunging pipes. This conclusion approximately holds for any compact source with a reasonably coherent magnetisation direction for which the external field is dominated by the dipole moment.

The total gradient $G(r)$ of the total magnetic field intensity $T(r)$ at an observation point $r = (x, y, z)$ is defined as follows:

$$G(r) = \sqrt{\left(\frac{\partial T(r)}{\partial x}\right)^2 + \left(\frac{\partial T(r)}{\partial y}\right)^2 + \left(\frac{\partial T(r)}{\partial z}\right)^2}. \quad \text{(Eqn 7.25)}$$

TG peaks towards the horizontal centre of a compact magnetisation and towards the margins of wider magnetisations, and Roest *et al.* (1992) demonstrated that it can be used to map the location of magnetisation contrasts.

7.3 SOURCES OF ERROR IN THE ANALYSIS

7.3.1 Imprecise location of the NSS peak

Our analysis depends on location of the horizontal centre of magnetisation. On any horizontal plane above a dipole the divergence of component and gradient ratios from the values estimated about its centre increases consistently with offset of the analysis from that centre. Figure 7.1 shows NSS contours over TMI images of low- and high-inclination magnetisations in a southern hemisphere geomagnetic field of inclination −60°. The TMI anomalies of these two magnetisations are quite different but the NSS anomalies are identical. Figure 7.2 plots the error in estimation of magnetisation direction from analysis of the field component ratios (Eqns 7.8 and 7.9). This error is zero directly above the dipole. For the low-inclination magnetisation the error increases most rapidly for azimuths parallel and anti-parallel to the declination of magnetisation (Fig. 7.2A). For the steep-inclination magnetisation there is less dependence on direction of the offset of the analysis (Fig. 7.2B) but in all directions the error increases more rapidly than for the low-inclination magnetisation. For the low-inclination magnetisation the error in estimating magnetisation direction is < 5° for horizontal errors of centre offset up to 10% of source depth, but for the steep magnetisation there is a threefold increase in this error. Gradient anomalies are sharper than their corresponding field anomalies and in consequence equivalent imprecision in locating the horizontal centre of an anomaly gives

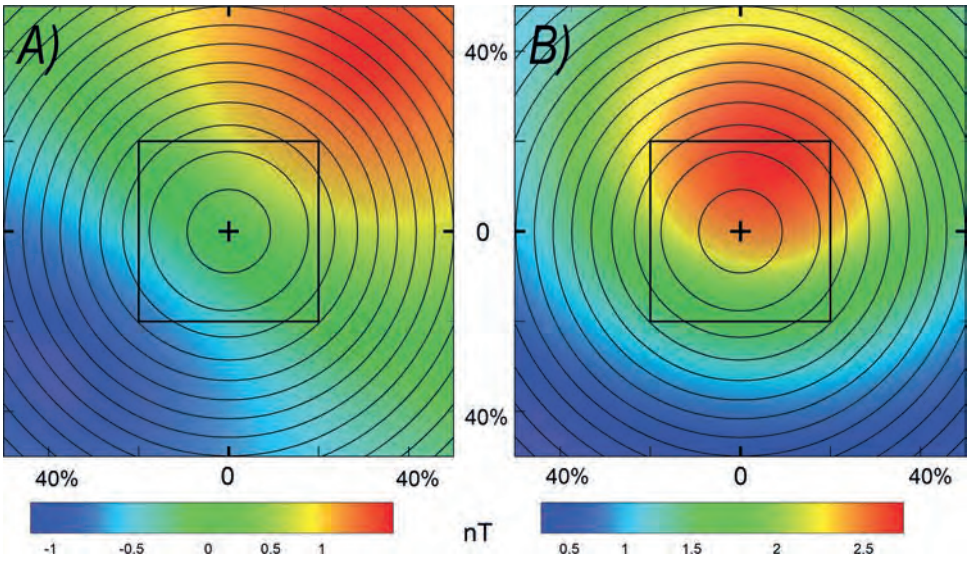

Fig. 7.1. NSS contours over TMI images for dipole magnetisations with declination 45° and inclination a) −15° and b) −75°. The horizontal scale is percentage of depth to the centre of magnetisation. The squares outline the area imaged in Fig. 7.2.

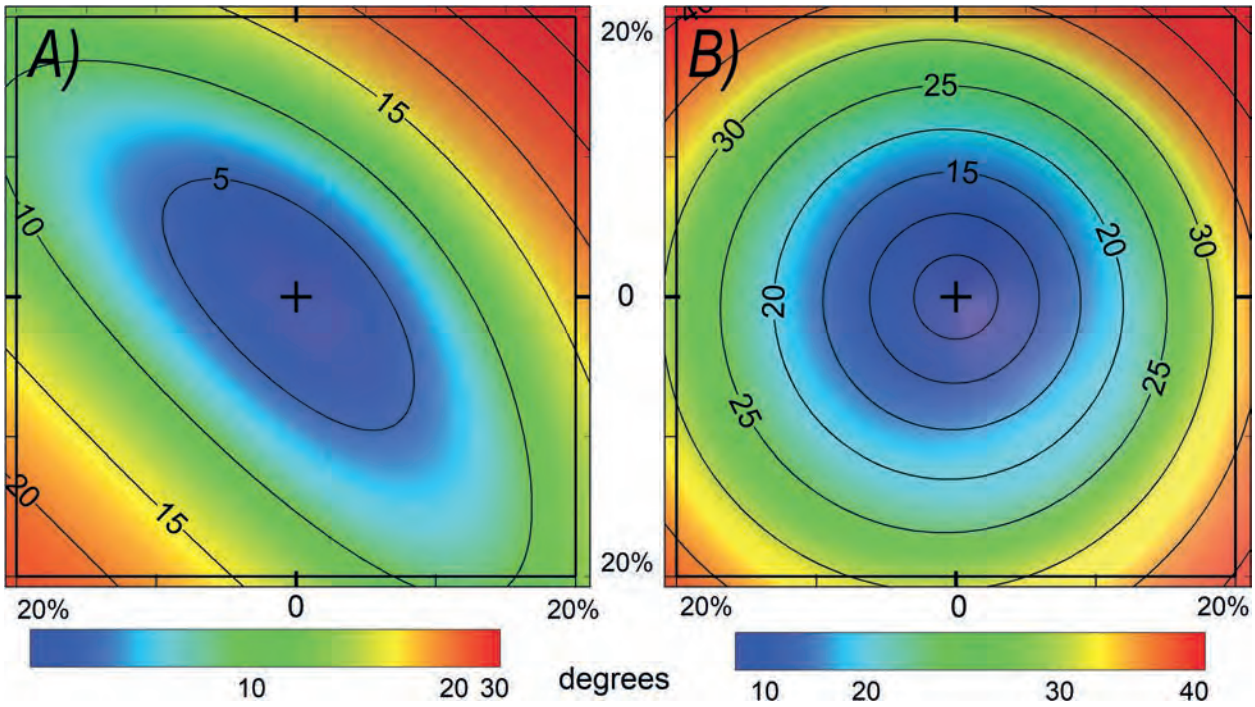

Fig. 7.2. Contoured error in magnetisation direction of the field component analysis for off-centred locations: a) low-inclination magnetisation (−15°) and b) steep-inclination magnetisation (−75°).

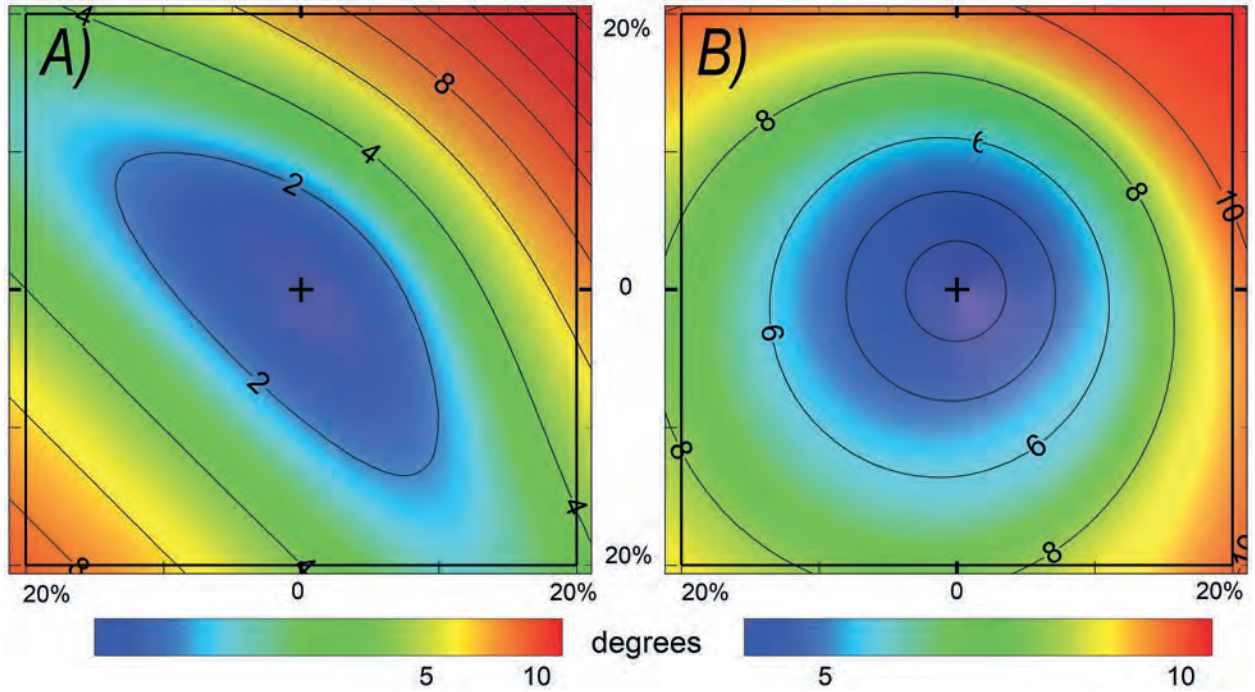

Fig. 7.3. Increase in error of magnetisation direction from the field component to the tensor gradient analysis for: a) low inclination (−15°) and b) steep inclination (−75°) magnetisations. Note that these errors are additional to those for the component analysis plotted in Fig. 7.2 and represent a penalty of using gradient rather than component analysis.

rise to larger errors in magnetisation direction from the gradient tensor analysis (Eqns 7.22 and 7.23) than from the component analysis (Eqns 7.8 and 7.9). Figure 7.3 plots the increase in error in changing from using component analysis to using gradient analysis. For location errors < 10% of source depth (the zone within which we hope the analysis will be performed) this increase is < 2° for the low-inclination magnetisation and < 5° for the steep-inclination magnetisation. We anticipate that in many cases this c. 30% loss of resolution from the use of gradients will be more than compensated by the advantage of lower sensitivity to the separation of the anomaly from its background field.

7.3.2 The influence of shape

Any departure from an ideal dipole compromises the model assumptions of relationships between magnetisation and the field or its gradients. For computations of non-dipole sources we have used expressions for the magnetic gradient tensor due to a uniformly magnetised general triaxial ellipsoid given in McKenzie (2020) and equations for the magnetic field components due to a uniformly magnetised general triaxial ellipsoid formulated in Clark *et al*. (1986). Figure 7.4 shows perspective views of several ellipsoids of axial ratios 1:1:0.5 and 1:0.5:0.5 and of centre depth to major axis length ratio 1:1. The departures of these bodies from dipoles distort the analysis in two ways: first the assumed dipole relationships are only approximate for these shapes, and second the NSS peak for these bodies may no longer mark their centre of magnetisation. We can investigate both effects by computing the dipole relationships over the known centre of magnetisation and at the NSS peak. We also include analysis at the alternative estimate of the centre of magnetisation provided by the total gradient transform. Results of these studies vary according to distribution shape and orientation of the magnetisation and its magnetisation direction.

Figure 7.5 is a map of error in a dipole tensor analysis. The figure shows an image of the angular difference between the input source magnetisation direction and the direction estimated by dipole tensor analysis (Eqns 7.22 and 7.23) from the magnetic field of an ellipsoid with horizontal north–south major axis of length 200 m, minor axes of 100 m, magnetisation inclination −75° and declination 45° and depth to centre 120 m. Note that for this non-dipole distribution of magnetisation there is a displacement between the centre of magnetisation (0,0) and the point at which by cancellation of errors the dipole tensor analysis provides the correct estimation of

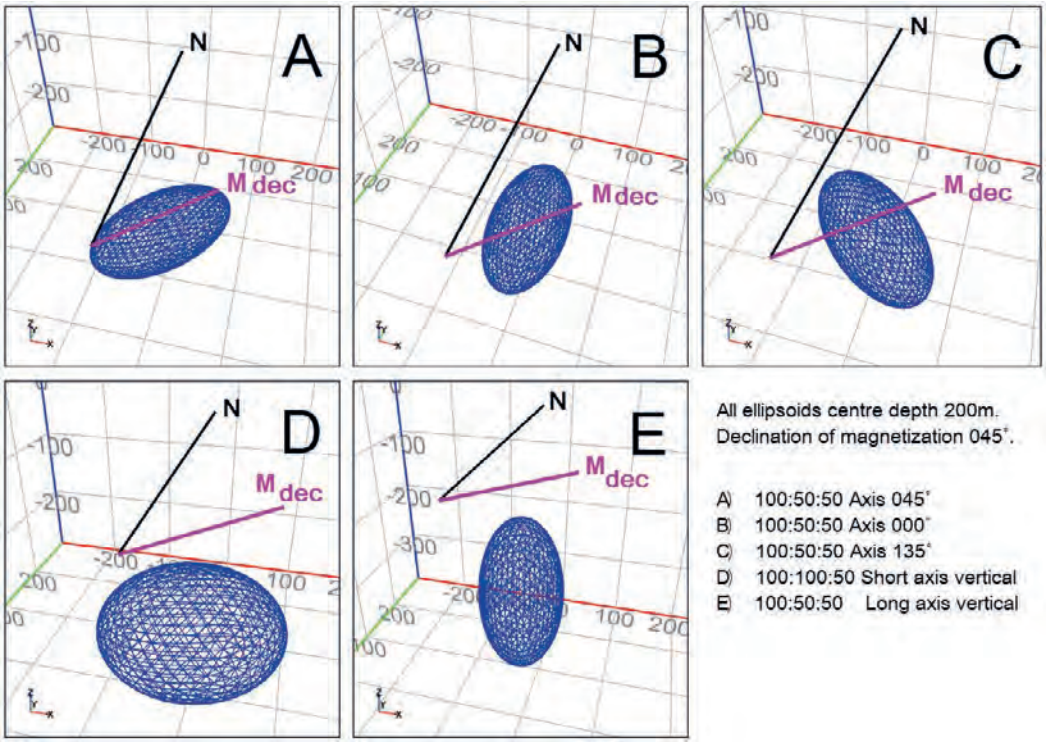

Fig. 7.4. Ellipsoids of different shape and orientation (but with horizontal and vertical axes) used to investigate the influence of shape in locating the centre of magnetisation and estimating magnetisation direction at those apparent centres.

magnetisation direction. Figure 7.5a shows the TG peak at which the tensor analysis has an error of 27°. Figure 7.5b shows a smaller displacement from the centre of magnetisation for the NSS peak at which the tensor analysis has an error of only 8° (Fig. 7.5b).

Figure 7.6 is a cross-plot of dipole component and tensor analysis errors for the various ellipsoids shown in Fig. 7.4. The symbols are shape coded to represent the various ellipsoid source models and colour coded to represent inclination of magnetisation. Tensor analysis at the NSS peaks has slightly larger error than component analysis. For the vertical ellipsoid (shown in Fig. 7.4E), flattened horizontal ellipsoid (shown in Fig. 7.4D) and ellipsoid with long axis perpendicular to the magnetisation direction (shown in Fig. 7.4C) both analyses have errors of less than 1°. Larger errors of up to 13° are found for various combinations of moderate- or steep-inclination magnetisations and ellipsoids with long axis perpendicular to the

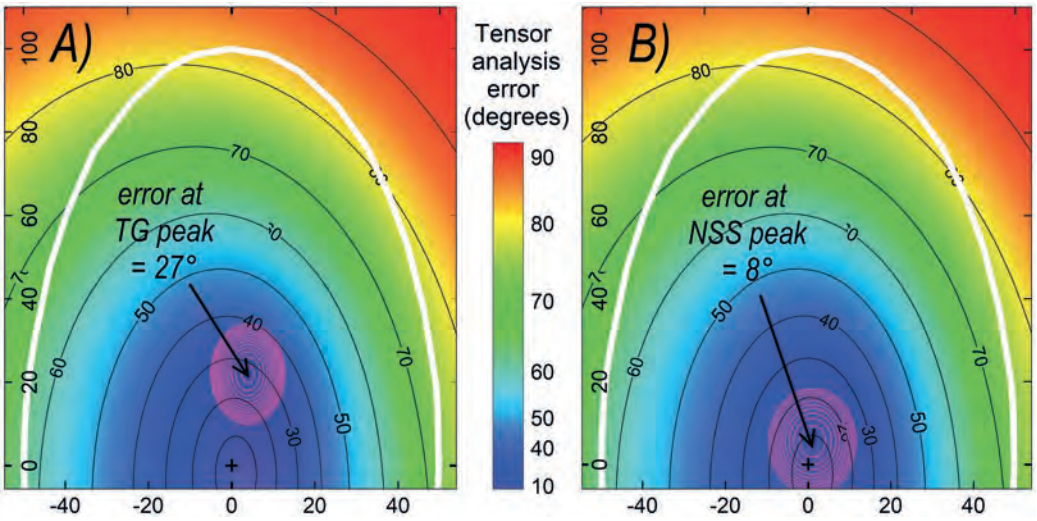

Fig. 7.5. Image of error in the tensor analysis of magnetisation direction overlaid by A) contours of the TG anomaly peak and B) contours of the NSS anomaly peak. The ellipsoid outline is shown in magenta.

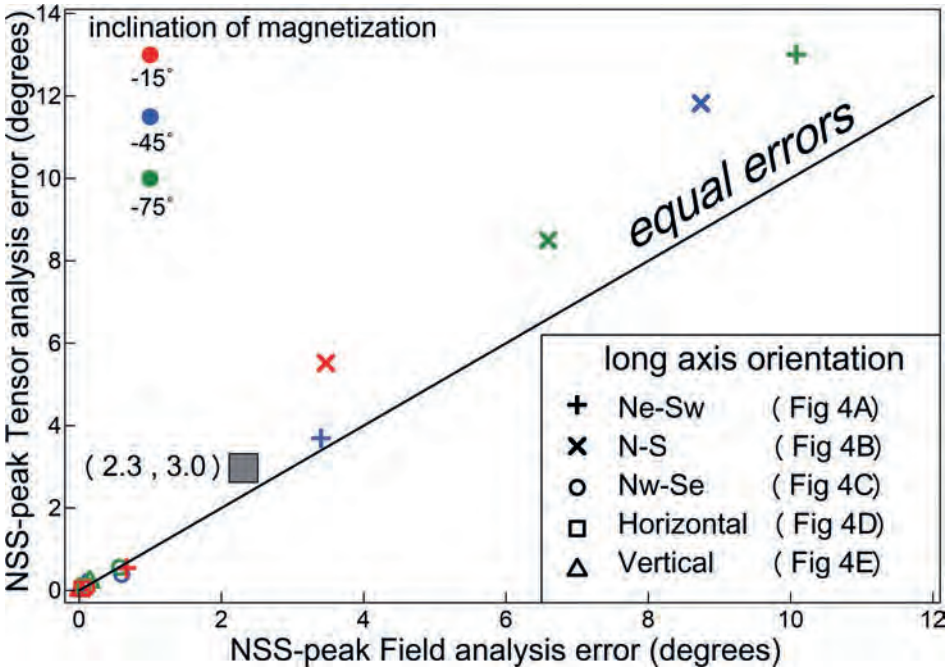

Fig. 7.6. Error in magnetisation direction at the NSS peak from tensor gradient and field component analyses for the ellipsoids show in Fig. 7.4. Note that many cases have low errors and plot in a cluster near the origin.

declination of magnetisation (shown in Fig. 7.4A) or at 45° to it (shown in Fig. 7.4B). Component and tensor analysis estimates of magnetisation direction have average errors of 2.3° and 3.0° respectively.

Figure 7.7 shows strong correlation between the displacement of the NSS peaks from the centre of magnetisation and the magnitude of error in magnetisation direction at those peaks estimated from the dipole tensor analysis. This strong correlation suggests that imperfect location of the centre of magnetisation is the dominant contribution to error in the analysis.

Figure 7.8 clearly shows the superiority of NSS over TG in estimating the centres of the various distributions of magnetisation. In all cases displacement of the TG

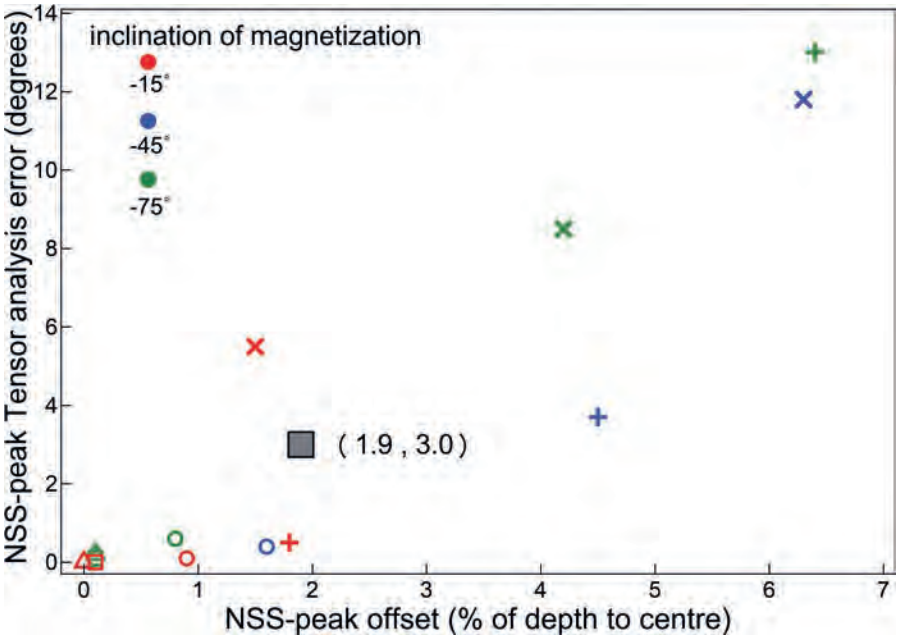

Fig. 7.7. Correlation of the offset of the NSS anomaly peak from the centre of magnetisation and the error in estimation of magnetisation direction by tensor gradient analysis at that peak. Symbols as in Fig. 7.6.

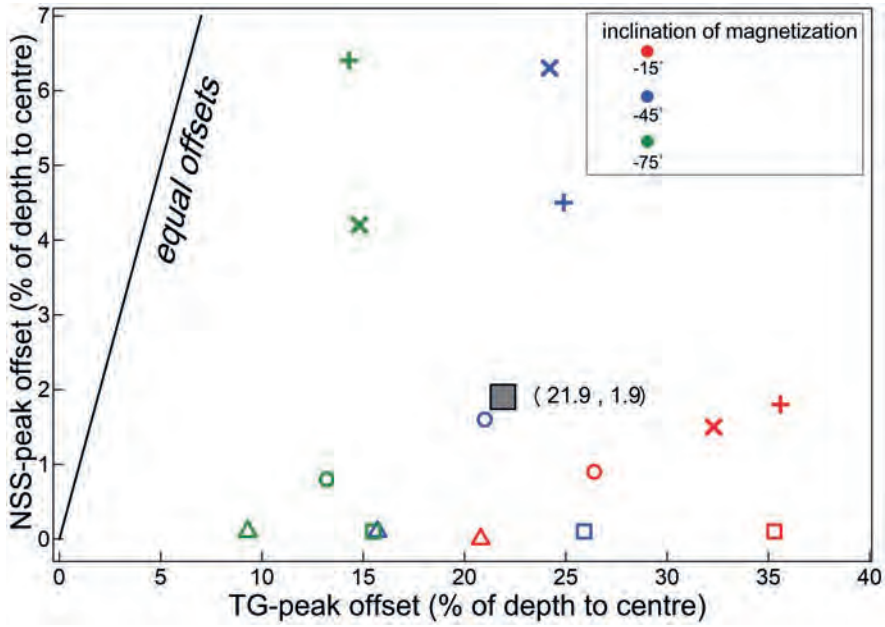

Fig. 7.8. Horizontal offset of the NSS and TG anomaly peaks from the centre of magnetisation. Symbols as in Fig. 7.6.

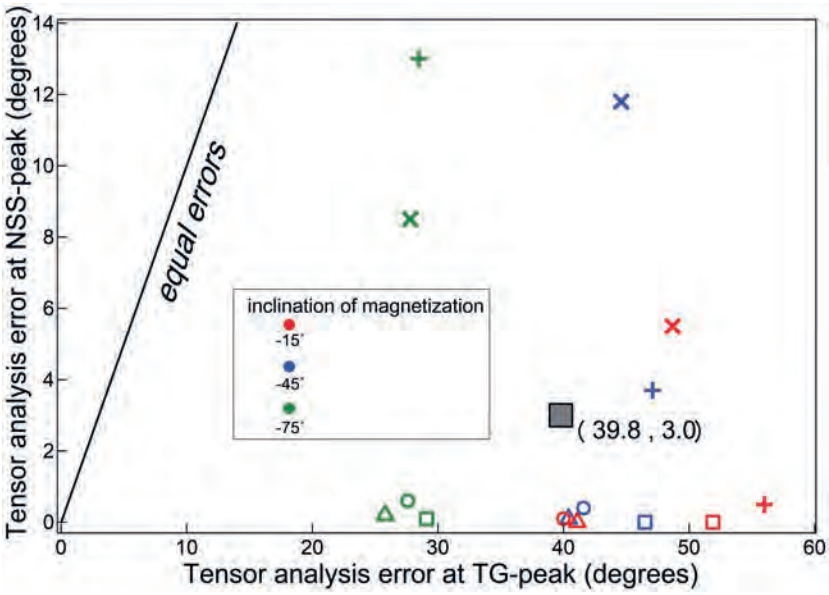

Fig. 7.9. Error in estimation of magnetisation direction by tensor gradient analysis at the NSS and TG anomaly peaks. Symbols as in Fig. 7.6.

peak is at least twice the displacement of the NSS peak. The average horizontal displacement of the NSS peak from the centre of magnetisation is 2% of depth to centre, and for the TG peak the average displacement is 20% of depth to centre. Consistent with our conclusion that error in locating the centre of magnetisation is the major source of error in the magnetisation analysis, corresponding errors in dipole tensor analysis at the NSS and TG peaks plotted in Fig. 7.9 follow a very similar pattern to offset of those peaks plotted in Fig. 7.8. The average error of the magnetisation analyses is 3° at the NSS peaks and 40° at the TG peaks.

7.3.3 The influence of plunge

For elongate thin sheet ('two-dimensional') magnetisations identical anomalies are produced by a wide range of interchangeable dip and inclination of magnetisation angles (Hood 1964). Ellipsoids best approximating segments of planar thin sheets ('plate' shapes) have a single short axis with plunge determined by the deviation of that short axis from the vertical. For ellipsoids with a single elongate axis ('cigar' shapes) plunge is determined by the deviation of the long axis from the horizontal. For a plunging source the shallower, up-plunge segment of the magnetisation produces higher amplitude, shorter wavelength contributions to the above-surface magnetic field than the deeper, down-plunge segment. This effect is most pronounced for plunging magnetisations of large depth extent. Plunge of a body is an intrinsic parameter, but if we consider it as secondary to other shape and position parameters we can recognise that in some circumstances the error in magnetisation direction due to plunge increases error due to other parameters and in other circumstances it reduces it. Plunge is therefore a complicating parameter. Figure 7.10 shows images of dipole tensor analysis error mapped for the magnetic fields of the same north–south elongated ellipsoid investigated in Fig. 7.5 but with a 15° plunge down to the north (Fig. 7.10a) and 15° down to the south (Fig. 7.10b). In each case the point at which dipole tensor analysis provides the correct magnetisation direction is shifted from the point above the centre of the ellipsoid towards the up-plunge direction. For this geometry, plunge and magnetisation direction, the TG peaks are further from the centre of magnetisation than the NSS peaks and in consequence the dipole tensor analysis error is larger at the TG peaks than at the NSS peaks. At the NSS peaks the dipole tensor analysis error (which was 8° for the horizontal body) is 5° (a change of −3°) for the northward plunge and 12° (a change of +4°) for the southward plunge. At the TG peak the error (which was 27° for the horizontal body) is 20° (a change of −7°) for the northward plunge and 34° (a change of +7°) for the southward plunge. These values vary with body shape, orientation, plunge, magnetisation direction and elevation at which the magnetic field is measured.

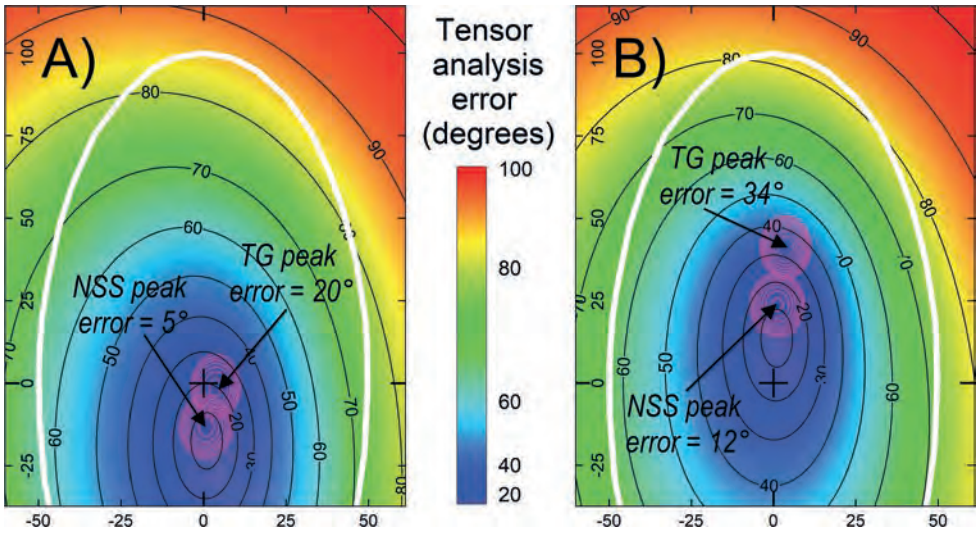

Fig. 7.10. NSS and TG peak contours over images of error in dipole tensor gradient analysis for the ellipsoid magnetisation of Fig. 7.5 with 15°plunge down a) to the north and b) to the south. The ellipsoid outline is shown in magenta.

7.3.4 The influence of elevation

The magnetic field expression of body shape and plunge varies with distance from the body, requiring the concept of 'compactness' (Clark 2014; Foss 2017; McKenzie 2020) to summarise the influence of these factors. One measure of compactness is the ratio between the longest axis of the body and distance to the closest measurement location, but no single statistic is sufficient to summarise the multi-factor variables describing the distribution of magnetisation and magnetic field measurements (see Chapter 4). At progressively greater distance the magnetic field of a body approximates closer to that of a dipole. Outside a spherical surface that entirely encloses an arbitrary magnetic source, the magnetic field can be described in terms of a multipole expansion (Jackson 2007, p. 145). Unless the dipole moment vanishes identically, the far-field is always dominated by the dipole term. For finite uniformly magnetised bodies of orthorhombic, or higher, symmetry (e.g. ellipsoids, rectangular prisms, right circular or elliptic cylinders) the quadrupole moment is zero and the lowest non-dipole term is usually the octupole contribution. As an extreme case, consider an axially magnetised long thin pipe, which behaves like a bar magnet with equal and opposite point poles at the ends. At a distance from the centre, r, that is greater than three times the length of the pipe, the non-dipole field in all directions contributes only ~5% of the dipole field, and this falls off as $\sim 1/r^2$ at greater distances. For sources that are more equidimensional, the dipole approximation is acceptable at shorter ranges than for an elongated source. For highly symmetric sources (cube, octahedron, cylinder with height/diameter ~0.9, etc.) the octupole term also vanishes and the source is well represented by a point dipole at relatively short ranges. For complex shapes such as pipes with horizontal top faces it may be convenient to separately consider a 'near-field' close to the source and a 'far-field' at greater distances, but for the ellipsoids which we have used in this study the influence of distance from source is more smoothly continuous. To investigate the influence of elevation at which the magnetic field is measured we computed the fields of a dipole and the same ellipsoid used in the study of plunge. NSS peaks directly above the dipole at all elevations and (as already proven) dipole tensor analysis at that peak exactly recovers magnetisation direction. For the dipole the TG peak has a consistent horizontal displacement from the magnetisation centre of 12% of its depth (Fig. 7.11a) and error of the dipole tensor analysis at that peak is consistently 27° (Fig. 7.11b). These values vary for different magnetisation directions and different geomagnetic field inclinations. For the north and south plunging ellipsoids NSS and TG peaks have almost converged to those of the otherwise identical horizontal ellipsoid at a depth of 400 m (twice the length of the longest axis). At this depth the dipole tensor analysis error for all three ellipsoids at their NSS peak is 8° and this reduces to 4° at a depth of 800 m. The dipole tensor analysis error for all three ellipsoids at their TG peak is ~27° across this depth range (the same as for the dipole).

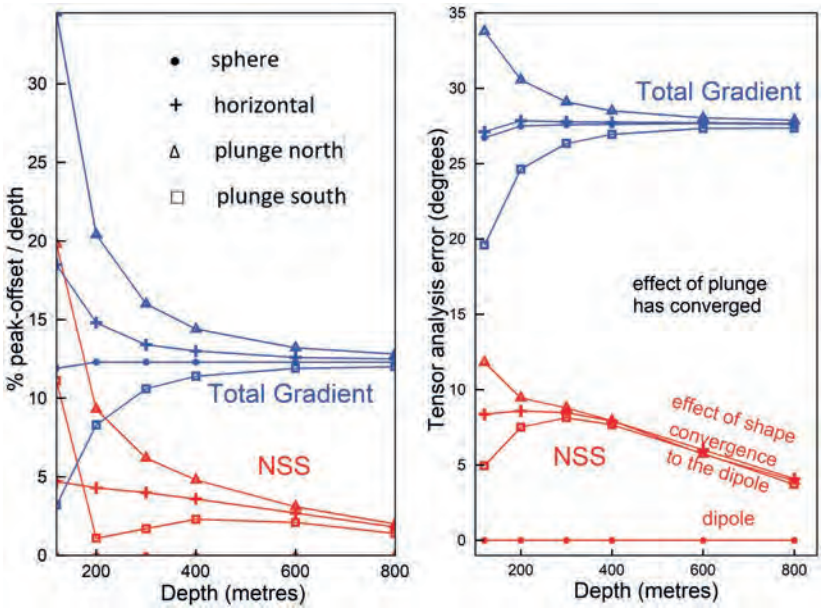

Fig. 7.11. a) NSS and TG peak offsets from the centre of magnetisation and b) error in dipole tensor magnetisation analysis at the NSS and TG peaks for a dipole and the ellipsoids of Figs 7.5 and 7.10.

An upward continuation of 100 to 200 m of the fields due to magnetisations at 120 m depth would reduce displacements of the NSS peak for the plunging ellipsoids with corresponding improvement of magnetisation direction estimates at those peaks. However, more substantial upward continuation is likely to achieve only slight further improvements due to substantial reduction in amplitude of the fields and gradients for these compact sources.

7.4 CASE STUDY

Figure 7.12a shows a measured TMI anomaly at Ethabuka, central Queensland, Australia from a survey with 400 m spaced east–west flightlines flown at a ground clearance of 80 m. There are no overlapping adjacent anomalies but there is some ambiguity in separating the anomaly from the background field. The east-south-east trough to peak orientation of this southern hemisphere anomaly indicates the declination of magnetisation, and the similar amplitudes of the peak and trough in this moderately steep geomagnetic field (inclination −65°) indicates a low inclination of magnetisation. Figure 7.12b shows an image of model-computed TMI for a parametric inversion of a steeply plunging elliptic cylinder (outline shown in Fig. 7.12b and 7.12c) with a top 740 m below sensor. The inversion simultaneously resolves the spatial and magnetisation properties of the model. The best estimated magnetisation direction is declination 100.8°, inclination +18.2°, consistent with expectations from visual analysis of the anomaly. The close match between the computed field in Fig. 7.12b and the measured field in Fig. 7.12a does not prove the inversion model correct but does justify it as at least an equivalent source suitable for use in data transforms. One such transform is an RTP using the recovered magnetisation direction, the output of which is shown in Fig. 7.12c. The compact positive-only RTP anomaly strongly supports the estimated magnetisation direction. The box in Fig. 7.12c is the area shown in greater detail in Fig. 7.13.

Figures 7.13a and 7.13b show TG and NSS peak contours over an image of the difference between magnetisation direction estimated by inversion and that computed at each grid cell using the tensor analysis algorithm. Tensor analysis at the NSS peak recovers an estimated magnetisation direction (completely independent of the inversion) only 5° different to the inversion estimate, and the NSS contours are closely co-centred with the RTP contours of Fig. 7.12c. The difference in estimated magnetisation direction between tensor analysis at the TG peak and the inversion result is 38°. Estimation of the location of magnetisation from the inversion model is also more compatible with the NSS peak than the TG peak. These relationships are further supported by almost identical results obtained by applying TG and NSS transforms to the model

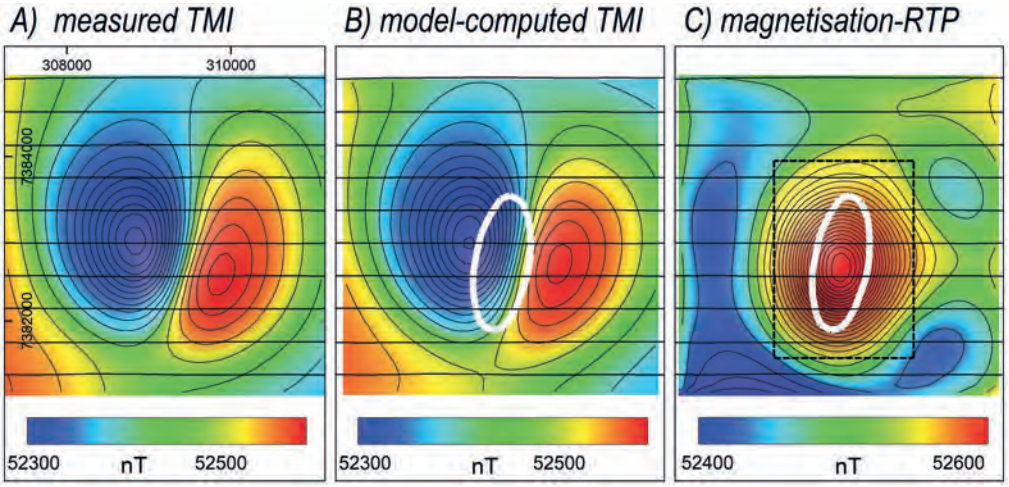

Fig. 7.12. The Ethabuka anomaly: a) measured TMI, b) model computed TMI with outline of the top of the model, and c) reduced to pole (RTP) TMI using the inversion model magnetisation direction.

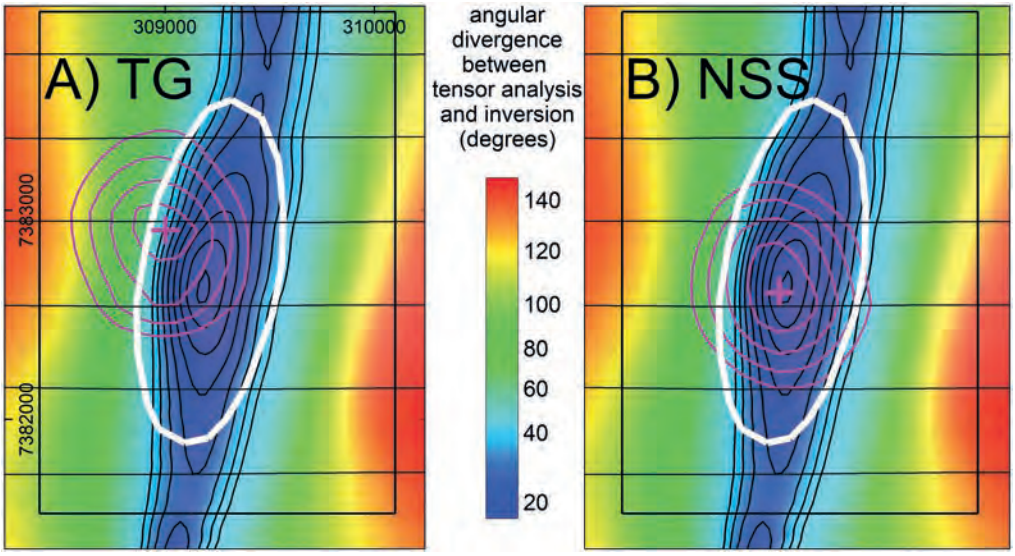

Fig. 7.13. Image and contour map (black with 5° contour interval) of the difference in magnetisation direction from inversion and tensor analysis with overlays (black lines) of a) TG peak contours and b) NSS peak contours. The outline of the inversion model is shown.

computed field of Fig. 7.12b for which the (virtual) magnetisation is of known direction and location.

7.5 CONCLUSIONS

We have shown that the direction of magnetisation of a dipole source can be derived from ratios of its field components or tensor gradient elements directly above its centre. The NSS transform peaks directly over a dipole and indicates where that analysis can be performed. The ratios of field components and of tensor gradients progressively diverge from their ideal values away from the centre axis of a dipole, and they also diverge for magnetisations which differ from a dipole. Estimates of magnetisation direction are particularly influenced by plunge. With increasing elevation the magnetic field of a compact source progressively converges towards that of an equivalent dipole, but any advantage of upward continuation to improve magnetisation estimates is restricted by attenuation of the magnetic field and gradients. We present a case study for which the NSS peak closely conforms with the centre of magnetisation derived by parametric inversion, and for which the magnetisation direction from dipole tensor gradient analysis at that peak agrees to within 5° of the inversion model. We only recommend dipole analysis for initial

magnetisation direction estimates. If magnetisation directions are required to higher precision they should be obtained by inversion, with a key advantage that inversion can be performed directly on the primary line data, avoiding any problems arising from gridding of the data.

REFERENCES

Beiki M, Clark DA, Austin JR, Foss CA (2012) Estimating source location using normalized magnetic source strength calculated from magnetic gradient tensor data. *Geophysics* **77**, J23–J37. doi:10.1190/geo2011-0437.1

Blakely RJ (1995) 'Potential theory in gravity and magnetic applications'. Cambridge University Press.

Caratori Tontini F, Pedersen LB (2008) 'Interpreting magnetic data by integral moments. *Geophysical Journal International* **174**, 815–824. doi:10.1111/j.1365-246X.2008.03872.x

Clark DA (2012) New methods for interpretation of magnetic vector and gradient tensor data I: eigenvector analysis and the normalised source strength. *Exploration Geophysics* **43**, 267–282. doi:10.1071/EG12020

Clark DA (2013) New methods for interpretation of magnetic vector and gradient tensor data II: application to the Mount Leyshon Anomaly, Queensland. *Exploration Geophysics* **44**, 114–127. doi:10.1071/EG12066

Clark DA (2014) Methods for determining remanent and total magnetisations of magnetic sources – a review. *Exploration Geophysics* **45**, 271–304. doi:10.1071/EG14013

Clark DA, Saul SJ, Emerson DW (1986) Magnetic and gravity anomalies of a triaxial ellipsoid. *Exploration Geophysics* **17**, 189–200. doi:10.1071/EG986189

Dannemiller N, Li Y (2006) A new method for determination of magnetization direction. *Geophysics* **71**, L69–L73.

Fedi M, Florio G, Rapolla A (1994) A method to estimate the total magnetization direction from a distortion analysis of magnetic anomalies. *Geophysical Prospecting* **42**, 261–274. doi:10.1111/j.1365-2478.1994.tb00209.x

Foss CA (2006) 'Evaluation of strategies to manage remanent magnetization effects in magnetic field inversion.' 76th Annual International Meeting, SEG, Expanded Abstracts, 938–942.

Foss CA (2017) 'Resultant-magnetisation based magnetic field interpretation' in V. Tschirhart and M.D. Thomas eds, Proceedings of Exploration 17: Sixth Decennial International Conference on Mineral Exploration, pp.637–648.

Foss CA, McKenzie KB (2011) Inversion of anomalies due to remanent magnetisation: an example from the Black Hill Norite of South Australia. *Australian Journal of Earth Sciences* **58**, 391–405. doi:10.1080/08120099.2011.581310

Fullagar PK, Pears GA (2015) 'Remanent magnetisation inversion.' 24th ASEG International Geophysical Conference, Extended Abstracts. doi:10.1071/ASEG2015ab188

Helbig K (1963) Some integrals of magnetic anomalies and their relation to the parameters of the disturbing body. *Zeitschrift für Geophysik* **29**, 83–96.

Hood P (1964) The Königsberger ratio and the dipping dyke equation. *Geophysical Prospecting* **12**, 440–456. doi:10.1111/j.1365-2478.1964.tb01916.x

Jackson JD (2007) 'Classical electrodynamics.' John Wiley & Sons.

Lelièvre PG, Oldenburg DW (2009) A 3D total magnetisation inversion applicable when significant, complicated remanence is present. *Geophysics* **74**, L21–L30. doi:10.1190/1.3103249

Li Y (2012) Recent advances in 3D generalized inversion of potential-field data. *SEG Technical Program Expanded Abstracts* **2012**, 1–7.

Lourenço JS, Morrison HF (1973) Vector magnetic anomalies derived from measurements of a single component of the field. *Geophysics* **38**, 359–368. doi:10.1190/1.1440346

McKenzie KB (2020) The magnetic gradient tensor of a triaxial ellipsoid, its derivation and its application to the determination of magnetisation direction. *Exploration Geophysics* **51**, 609–641. doi:10.1080/08123985.2020.1726176

McKenzie KB, Foss CA, Hillan D (2012) 'An improved search for magnetisation direction.' 22nd ASEG Geophysical Conference, Extended Abstracts, 1–4.

Paine J, Haederle M, Flis M (2001) Using transformed TMI data to invert for remanently magnetised bodies. *Exploration Geophysics* **32**, 238–242. doi:10.1071/EG01238

Phillips JD (2005) Can we estimate total magnetisation directions from aeromagnetic data using Helbig's integrals? *Earth, Planets, and Space* **57**, 681–689. doi:10.1186/BF03351848

Phillips JD, Nabighian MN, Smith DV, Li Y (2007) Estimating locations and total magnetisation vectors of compact magnetic sources through combined Helbig and Euler analysis. *SEG Technical Program Expanded Abstracts* **26**, 770–774.

Pratt DA, McKenzie KB, White AS (2014) Remote remanence determination (RRE). *Exploration Geophysics* **45**, 314–323. doi:10.1071/EG14031

Purucker ME (1990) The computation of vector magnetic anomalies: A comparison of techniques and errors. *Physics of the Earth and Planetary Interiors* **62**, 231–245. doi:10.1016/0031-9201(90)90168-W

Roest WR, Verhoef J, Pilkington M (1992) Magnetic interpretation using the 3-D analytic signal. *Geophysics* **57**, 116–125. doi:10.1190/1.1443174

Schmidt PW, Clark DA (1998) The calculation of magnetic components and moments from TMI: a case study from the Tuckers igneous complex, Queensland. *Exploration Geophysics* **29**, 609–614. doi:10.1071/EG998609

Wilson HS (1985) 'Analysis of the magnetic gradient tensor.' Defence Research Establishment Pacific, Technical Memorandum **8**, 5–13.

Wynn WN, Frahm CP, Carroll PJ, Clark RH, Wellhoner J, Wynn MJ (1975) Advanced superconducting gradiometer/magnetometer arrays and a novel signal processing technique. *IEEE Transactions on Magnetics* **11**, 701–707. doi:10.1109/TMAG.1975.1058672